

INVESTIGATION OF THE EFFECT OF DIFFERENT DESIGN AND FLOW PARAMETERS ON BATTERY COOLING SYSTEM PERFORMANCE

Ersel DÖNMEZ *^{ID}
Emre BULUT *^{ID}

Received: 19.10.2024; revised: 24.11.2024; accepted: 26.11.2024

Abstract: In this study, a module consisting of 30 pouch-type lithium-ion batteries with Lithium Iron Phosphate (LFP) chemistry, known for its lower flammability, was modeled along with its cooling system in a one-dimensional framework. The modeling was conducted using MATLAB Simulink and Simscape Battery. The temperature variations and heat generation rates of the battery system were analyzed at different discharge rates. A liquid cooling system, designed to cool the battery module from below, was developed. The cooling performance was examined by selecting a laminar flow regime at lower Reynolds numbers, which was assumed to result in lower pumping losses. In the analyses performed at different Reynolds numbers and with varying numbers of cooling plate channels, it was observed that as the Reynolds number increased, both the heat transfer rate and coolant flow velocity increased, leading to a reduction in battery temperature values but an increase in pressure values.

Keywords: Battery cooling system, 1-D modelling, Lithium-ion battery

Farklı Tasarım ve Akış Parametrelerinin Batarya Soğutma Sistemi Performansına Etkisinin İncelenmesi

Öz: Bu çalışmada elektrikli araçlarda kullanılan, yanıcılığı daha az olan Lityum Demir Fosfat kimyasına sahip, 30 adet kese (pouch) tipi adı verilen Lityum iyon bataryadan oluşan bir modül ve soğutma sistemi bir boyutlu olarak modellenmiş ve soğutma performansı incelenmiştir. Modelleme MATLAB Simulink ve Simscape Battery ortamında gerçekleştirilmiştir. Farklı deşarj oranlarında batarya sisteminin sıcaklık değişimleri ve ısı üretim miktarları incelenmiştir. Batarya modülünü soğutabilmek için, alttan olacak şekilde sıvı soğutma sistemi tasarlanmıştır. Sıvı soğutma sisteminde pompalama kayıplarının daha az olduğu düşünülen daha düşük Reynolds sayılarında laminer akış tipi seçilerek soğutma performansı incelenmiştir. Farklı Reynolds sayılarında ve farklı soğutma plakası kanal sayılarında yapılan analizlerde, Reynolds sayısı arttıkça ısı transfer hızı ve soğutma sıvısı hızı arttığı için batarya sıcaklık değerlerinde düşüş ve basınç değerlerinde artış görülmüştür.

Anahtar Kelimeler: Batarya soğutma sistemi, Bir boyutlu modelleme, lityum iyon batarya

* Bursa Uludağ Üniversitesi, Mühendislik Fakültesi, Otomotiv Mühendisliği Bölümü, Görükle Kampüsü, 16059 Bursa
Correspondance Author: Emre Bulut (ebulut@uludag.edu.tr)

1. INTRODUCTION

Given the significant advantages of Li-ion batteries, their application has become increasingly widespread with ongoing advancements. These batteries are utilized in various sectors, including electric vehicles, consumer electronics such as mobile devices, household appliances, and energy storage systems in military equipment. Based on their physical characteristics, Li-ion batteries can be categorized into pouch, cylindrical, and prismatic types. However, if a battery is charged or discharged at a high C rate without an adequate cooling system, overheating and thermal runaway may occur. It is crucial to minimize excessive temperature variations within the battery. Ideally, the maximum temperature difference should not exceed 5 °C (Fu et al., 2023).

If we look at the historical development of lithium-ion batteries, in 1987, Akira Yoshino reported a lithium-ion battery design based on a LiCoO₂ cathode and carbonate ester electrolyte. He was the first to commercialize a battery that used a soft carbon anode (a coal-like material) and electrolyte, and he patented this lithium-ion battery. The design featured a hollow structure, which enhanced production safety and reduced costs. In 1991, Sony utilized Yoshino's design to produce and sell the world's first rechargeable lithium-ion batteries. The following year, a joint venture between Toshiba and Asahi Kasei launched further developments in lithium-ion battery technology (Li et al., 2018). In the 1990s, the soft carbon anode was first replaced with hard carbon and later with graphite, leading to significant improvements in energy density (Fong, Sacken et al., 1990). In April 2023, CATL announced a breakthrough in solid-state battery technology, achieving a record energy density of 500 Wh/kg. This development marks a significant increase in the production capacity of solid condensed batteries. The new design employs electrodes without binders and features a gelled accumulator, resulting in reduced production downtime (Hanley, 2023).

Ghiji et al., (2020) determined that thermal runaway poses a significant fire hazard, particularly in enclosed spaces. Over the past 20 years, there have been more than 300 fires associated with Li-ion batteries, highlighting the serious safety risks these batteries can present. The causes of these incidents include battery overheating, internal short circuits, short circuits during charging, sudden battery ignition, loose connections leading to overheating, short circuits due to water exposure, short circuits in battery modules during collisions, and gas release followed by ignition. These issues often arise from short circuits between the positive and negative terminals. Graphite is the most used anode material in lithium-ion batteries and is expected to remain so for the next few decades (Zhang et al., 2021). Yu et al. (2024) investigated thermal runaway mechanisms of a NCA-graphite lithium-ion battery and reported that graphite anode + electrolyte reactions contribute 53.8% of the total heat.

Since thermal runaway is one of the most critical issues in battery modules, researchers worldwide had been investigating various battery cooling systems. Monika et al. (2022) compared different channel structures in their study, focusing on enhancing cooling efficiency. They found that parallel and serpentine channels, commonly used in traditional designs, were gradually replaced by alternative channels with improved cooling performance. The researchers designed six cold plates with identical channel volumes: straight channels, serpentine channels, U-shaped channels, gourd-shaped channels, spiral channels, and hexagonal channels. In their numerical analysis, despite higher pressure drops, the serpentine and hexagonal channels demonstrated superior cooling properties. The temperature distribution in the battery system was significantly improved with these designs.

Batteries can reach high temperatures when operating at high performance, and if not adequately cooled, this can cause structural damage and render the battery unusable. To prevent this, a battery thermal management system (BTMS) is essential. BTMS can utilize either passive cooling—relying solely on ambient temperature—or active cooling, where devices are integrated into the cooling medium. Most cooling systems employ external cooling techniques, where heat is removed from the battery surface. Therefore, it is crucial to maintain an effective cooling

system to keep the batteries within a specific temperature range, ensuring optimal performance and longevity.

Simulating and predicting the heat generation and heat dissipation is important for designing BTMSs. Although lots of researchers are present in the literature, most of the simulations are benefiting the 3D- (Computational Fluid Dynamic) CFD Tools. There are few studies employes 1D electrical and thermal models and cooling systems (Kim et al., 2023; Kumar et al., 2023). In this study, a 1D battery model was developed using MATLAB Simulink Simscape software, and the temperature values obtained from the model at different discharge rates (2C, 3C, 4C) were compared with data from the literature. Since pressure drop increases the parasitic power absorbed from the battery system, laminar flow within the cooling channels is preferred. The cooling performance of the system is analyzed under 4C discharge conditions, focusing on cooling scenarios with different Reynolds numbers within the cooling channels, aiming to provide valuable contributions to other researchers.

2. MATERIAL AND METHOD

2.1. One Dimensional Battery Cooling System with Parallel Channels

In this section, MATLAB Simscape Battery and Simulink are used for one-dimensional modeling software. At different discharge rates (2C, 3C, 4C) the battery heat generation and the temperature values are validated with the results in the literature. Different liquid cooling systems with parallel channels are designed to cool the battery module from bottom of the module.

2.1.1. Li-Ion Battery Technical Specifications

In this study, a battery with Lithium Iron Phosphate (LFP-LiFePO₄) chemistry, AMP20M1 HD from the A123 brand, is selected. The specifications of the battery used are given in Table 1.

Table 1. Technical specifications of the selected battery (A123, AMP20M1HD-A, 2011)

Brand	A123 system
Model	AMP20M1HD
Chemistry	LFP-LiFePO ₄
Voltage	3.3V (nominal)
Capacity	19.6 mAh
Dimension	7.25 x 160 x 227
Weight	496 g
Operating Temperature	-30 °C – 55 °C
Storage Temperature	-40 °C – 60 °C

The modeling is performed in the MATLAB Simulink and Simscape Battery environment. This platform allows for the development and evaluation of various battery pack architectures, enabling the assessment of their performance under different conditions.

2.1.2. Battery Model Equations

The discharge rate must be considered in the calculations. The capacity of the cell is 20 Ah, meaning that if a current of 20A is drawn, the cell will be fully discharged in one hour. If the C-rate is taken as 2, which corresponds to the nominal value of the battery, the discharge current would be 40A, as the capacity is 20 Ah. The C-rate equation is provided in Equation 3.1, and the equation for calculating the expected usable time of the battery is presented in Equation 3.2.

$$C \text{ rate} = \frac{\text{Charge or discharge current}}{\text{Battery nominal capacity}} \quad (1)$$

Here, C rate is the charging or discharging rate against the charging or discharging current (A). It is obtained by dividing it by its capacity (Ah).

$$\text{Hour} = \frac{\text{Discharge capacity}}{\text{Discharge current}} \quad (2)$$

The modeling is conducted without a cooling system for validation with the addition of key components such as the MATLAB battery cell, discharge, step function, Simulink-PS converter, and grounding blocks. The Simulink model is illustrated in Figure 1. The model consists of a discharger block for discharge the battery with constant current, PS Step signal for triggering the discharger block, temperature source block for ambient temperature input, battery, electric reference and solver configuration blocks.

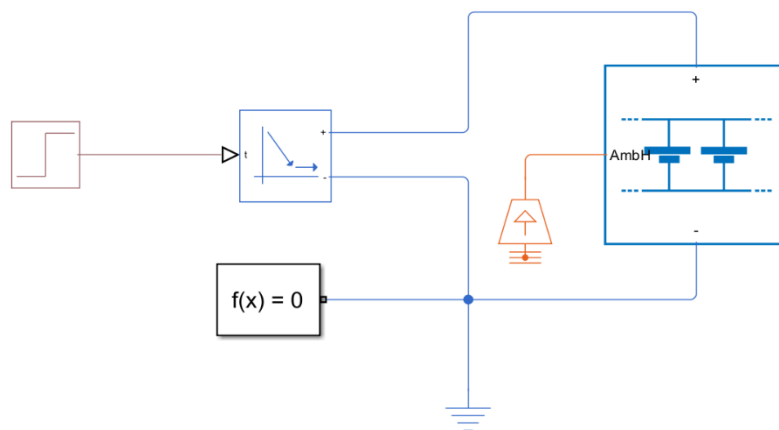


Figure 1:
One dimensional battery model without cooling system

The model is established and run without a cooling system at different discharge rates. The battery equivalent block calculates the total battery heat generation rate by adding the following expression is shown in Equation 3 (Bernardi et al., 1985).

$$\dot{Q}_{gen} = P_{diss} + \dot{Q}_{rev} + \dot{Q}_{flow,exr} \quad (3)$$

P_{diss} is the power loss term of all resistors in the equivalent circuit topology. The irreversible heat generation due to battery polarization can be neglected be calculated with Equation 4.

$$P_{diss} = I^2 R_0 \tag{4}$$

Here, I is the current [A] and R_0 is the instantaneous resistance of the battery cell.

\dot{Q}_{rev} is the reversible heat generation from entropy and can be calculated with Equation 5.

$$\dot{Q}_{rev} = IxTx \frac{dOCV}{dt} \tag{5}$$

Where OCV is the Open Circuit Voltage and T is the temperature.

$\dot{Q}_{flow,exr}$ comes from faulty cell behaviour such as short circuit, open circuit resistance and thermal runaway heat of reaction concepts.

The temperature variations at different discharge rates are validated using experimental data from a study in the literature that employed the same battery (Panchal et.al, 2014). The temperature changes from both the simulation and experimental data are presented in Figure 2.

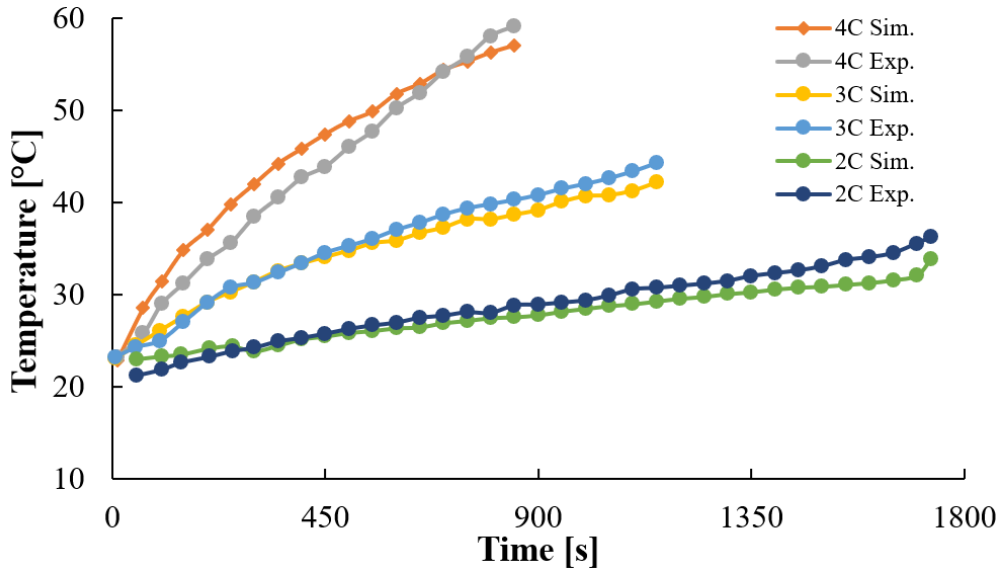


Figure 2:
Experimental and simulated temperature values at different C rates

2.1.3. Modelling of The Battery Module

For the model with a cooling system, components such as a reservoir, flow source, and a parallel-channel cooling plate are added. The cooling plate is used to regulate the temperature of the battery module. Thermophysical properties of water, battery and aluminum sheet are given Table 2. The flow source ensures fluid flows at specific mass flow rates, while the reservoir supplies the necessary fluid to the system. The design and the model of the battery cooling system is illustrated in Figure 3.

The conductive heat transfer between cooling plate and battery module is calculated by using Equation 6 (Çengel, 1998).

$$Q = kA \frac{dT}{dX} \quad (6)$$

Where T is the temperature, k is the thermal conductivity of the plate, and A and x depend on the plate thickness and on the number of partitions and directions, x or y .

The heat flow rate between the thermal liquid and the cooling channels walls is shown in Equation 7.

$$Q_H = Q_{conv} + \frac{kS_H}{D}(T_h - T) \quad (7)$$

Q_h is the net heat flow rate, Q_{conv} is the heat flow rate from convection. k is the thermal conductivity of the thermal liquid in the cooling channel. S_h is the surface area of the cooling channel wall, the product of the cooling channel perimeter and length. T_h is the temperature at the cooling channel wall.

For an exponential temperature distribution along the cooling channel, the convective heat transfer can be calculated with Equation 8.

$$Q_{conv} = |\dot{m}_{avg}|c_{p,avg}(T_H - T_{in}) \left(1 - \exp\left(-\frac{h_{coeff}S_H}{|\dot{m}_{avg}|c_{p,avg}}\right) \right) \quad (8)$$

\dot{m}_{avg} is the average mass flow rate. $c_{p,avg}$ is the specific heat evaluated at the average temperature. T_{in} is the inlet temperature depending on flow direction.

The heat transfer coefficient, h_{coeff} , depends on the Nusselt number shown in Equation 9.

$$h_{coeff} = Nu \frac{k_{avg}}{D} \quad (9)$$

D is the hydraulic diameter of the pipe.

In Equation 10 is shown pressure calculation (White and Xue, 2003).

$$p = f2 \frac{L\rho v^2}{D} \quad (10)$$

p is the pressure in Pascal. f is the Darcy factor in laminar flow. L in meters is the length. ρ is the density [kg/m³], v is the velocity and expressed m/s. D is the diameter expression in meters.

Table 2. Thermophysical properties of the battery, aluminium and water (Bulut et al., 2021; Lin et al., 2022)

Material	ρ [kg/m ³]	c_p [J/(kgK)]	K [W/(mK)]	μ [Pa.s]
Battery	2092	900	18.2	-
Aluminium	2719	871	202.4	-
Water	998.2	4182	0.6	0.001

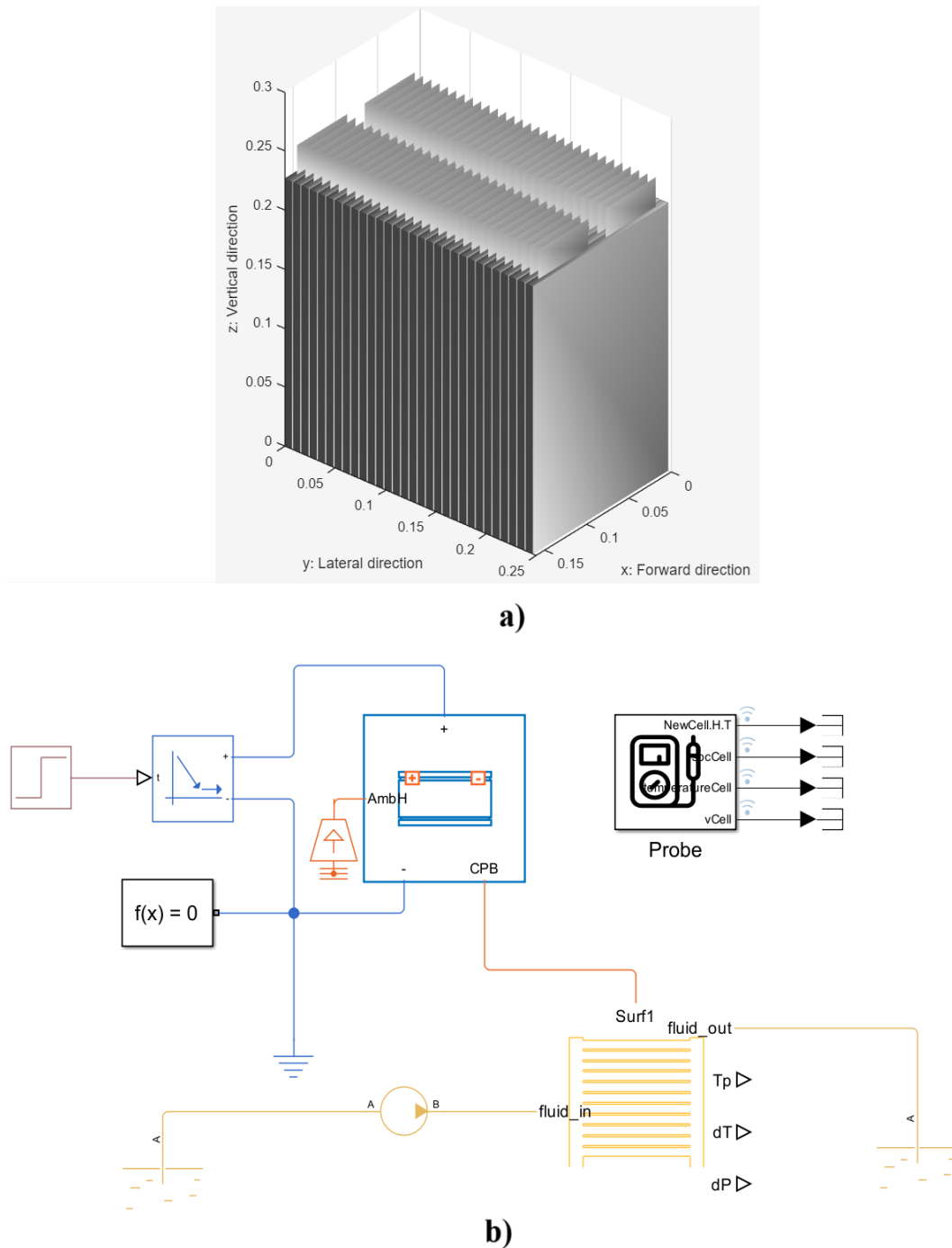


Figure 3:
a) Design of the battery module b) Simulink model of the battery module with cooling system

3. RESULTS AND DISCUSSION

The pressure drop characteristics of the cooling system are evaluated for varying Reynolds numbers (200, 300, 400, 1000, 1500, and 2000) and different numbers of cooling channels. Figure 4 illustrates the pressure drop at Reynolds numbers 200, 300, and 400 for various channel configurations. It can be seen that, as the number of channels increases, the pressure drop rises

steadily. At lower Reynolds numbers (200, 300, 400), the pressure drop values increase from approximately 150 Pa to around 450 Pa as the number of channels grows from 4 to 8. This can be attributed to the increased number of bends in the cooling channel distributor and collector, as well as the increasing mass flow rate, which leads to increasing pressure drop due to friction and local losses.

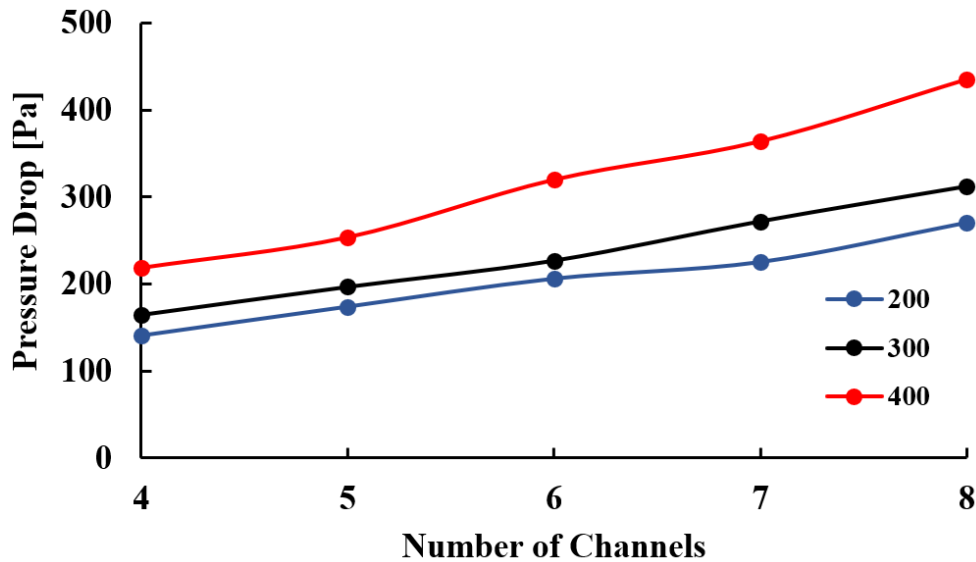


Figure 4:
Pressure drop values for Reynolds 200,300 and 400 at different number of channels

The analyses for Reynolds numbers 200, 300, and 400 are conducted by maintaining the flow regime in the laminar zone, where the flow remains steady and predictable. As the number of channels increases, the system's overall flow rate increases as well, which leads to a corresponding increase in pressure drop. However, this pressure drop remains relatively moderate within the laminar flow regime, which does not yet exhibit the turbulence-induced escalations seen at higher Reynolds numbers.

In contrast, Figure 5 presents pressure drop results for Reynolds numbers 1000, 1500, and 2000 across different channel numbers. For higher Reynolds numbers, the pressure drop increases significantly, especially when the number of channels is raised, due to increase in the mass flow rate of the system. As the Reynolds number increases, the flow transitions from laminar to turbulent. At Reynolds numbers 1000, 1500, and 2000, the pressure drop increases sharply, reaching values between 6000 Pa and 24000 Pa as the number of channels increases. This phenomenon is due to the onset of turbulence, where turbulent flow results in higher frictional losses, demanding more energy to pump the coolant through the system.

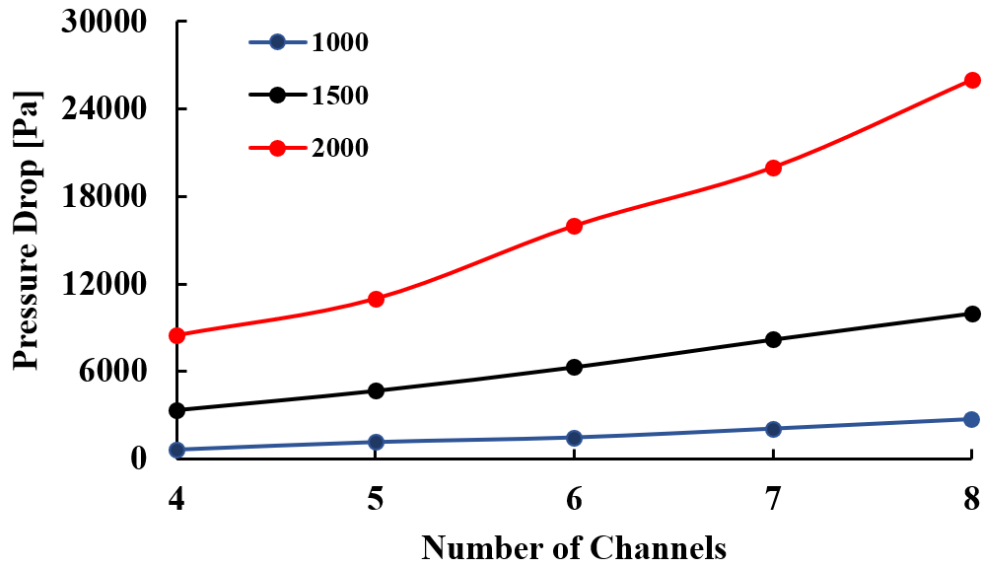


Figure 5:
Pressure drop values for Reynolds 1000, 1500 and 2000 at different number of channels

This shift from laminar to turbulent flow highlights a key challenge in cooling system design: while additional channels can increase the available heat transfer surface area, they also introduce significant pressure drop in turbulent flow conditions.

The cooling performance of the system is also evaluated by analyzing the maximum temperature at various Reynolds numbers and channel configurations. In the absence of cooling, the maximum temperature of the battery module reached 334 K. The maximum temperature values for Reynolds numbers 200, 300, 400, 1000, 1500, and 2000, under different channel configurations are shown in Figure 6.

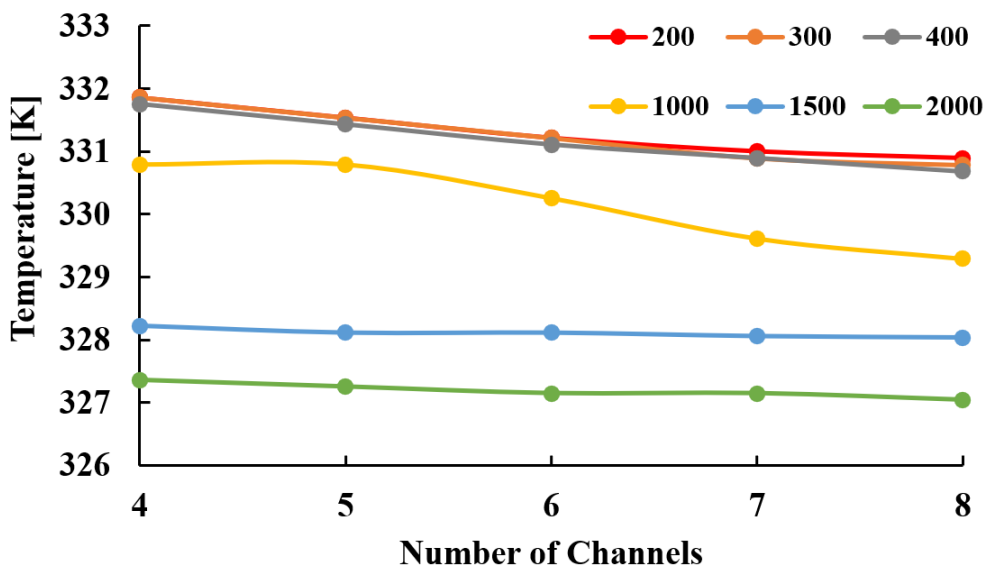


Figure 6:
Temperature values at different number of channels for different Reynolds Number

Figure 6. demonstrates that the cooling performance improves with an increase in both the Reynolds number and the number of cooling channels, although the effect of adding more channels diminishes as the Reynolds number increases. At low Reynolds numbers (200, 300 and 400), the cooling effect from increasing channels is moderate, while at higher Reynolds numbers (1000, 1500 and 2000), the cooling system stabilizes at lower temperatures, and further increasing the number of channels has a limited impact. This suggests that for optimal thermal management in the battery cooling system, both the flow rate (Reynolds number) and the channel configuration should be considered to balance cooling efficiency and design complexity.

Furthermore, while increasing the number of channels can enhance cooling performance in the laminar flow regime, the effect diminishes at higher Reynolds numbers. Qian et al. (2016) reported that increase in the number of channels can decrease the maximum temperature values and, they found a 5-channel cooling plate is enough. The further decrease in temperature, they suggested increasing the mass flow rate. They also reported that, for constant mass flow rate, increasing the number of channels reduces the pressure drop. A fewer number of channels will both increase the pressure drop and deteriorate the cooling performance. Therefore, the design of cooling systems should aim for a balance: optimizing the number of channels and flow parameters to improve heat dissipation while accounting for the pressure losses introduced by additional channels, particularly in turbulent flow conditions.

4. CONCLUSION

In this study, a one-dimensional model of a Li-ion battery module and cooling system, consisting of 30 pouch-type LFP cells (AMP20M1 HD), was developed, and its liquid cooling performance was investigated.

- First, a one-dimensional model of the battery was created without a cooling system. The analysis revealed that the temperature reached around 334 K. It was seen that as the discharge rate increased, the temperature values increased.
- The effect of the number of channels on the pressure drop was investigated, revealing that as the number of channels increased, pressure drop values varied between 150 and 450 Pa, especially for Reynolds numbers of 200, 300, and 400. This was attributed to the increased number of bends in the system, coupled with the rise in mass flow rate. Additionally, as Reynolds numbers increased, the system transitioned from laminar to turbulent flow, leading to a sharp rise in pressure drop, particularly for Reynolds numbers of 1000, 1500, and 2000.
- In the cooling system analysis performed at Reynolds 200, 300, 400, 1000, 1500 and 2000 values, the system temperature of 332 K at Reynolds 200 decreased to 327 K at Reynolds 2000 value. The cooling capacity for the laminar flow zone has reached a sufficient level.
- While the number of channels has been increased, the channel width was constant and the effect of the channel width on cooling system performance will be further investigated in future studies, particularly under high discharge rates in the laminar flow regime. An optimization study with the channel width, the number of channels and the mass flow rate parameters will contribute to the literature even more comprehensively.
- In the cooling system analysis conducted at Reynolds numbers of 200, 300, 400, 1000, 1500, and 2000, the system temperature decreased from 332 K at Reynolds

200 to 327 K at Reynolds 2000. The cooling capacity in the laminar flow regime can be insufficient for safe operation.

- This study examines the performance of the cooling system under laminar flow conditions, where pressure losses are lower, since the higher pressure losses can increase the power consumption of the battery cooling systems in electric or hybrid vehicles. Design engineers should consider this carefully that increasing the number of channels raises the mass flow rate of system, which may lead to turbulent flow in the distributor and collector sections.

CONFLICT OF INTEREST

The authors declare no conflicts of interest.

AUTHOR CONTRIBUTION

Emre Bulut and Ersel Dönmez determining the concept and design process of the research and research management, Ersel Dönmez data collection and analysis, Emre Bulut and Ersel Dönmez data analysis and interpretation of results.

REFERENCES

1. A123, (2024) Access address: <https://www.buaya123products.com/uploads/vipcase/468623916e3ecc5b8a5f3d20825eb98d.pdf> Access date:20.09.2024
2. Bernardi, D., Pawlikowski, E., & Newman, J. (1985). A general energy balance for battery systems. *Journal of The Electrochemical Society*, 132(1), 5. doi:10.1149/1.2113792
3. Bulut, E., Albak, E. I., Sevilgen, G., & Öztürk, F. (2021). A new approach for battery thermal management system design based on grey relational analysis and latin hypercube sampling. *Case Studies in Thermal Engineering*, 28, 101452. doi:10.1016/j.csite.2021.101452
4. Cengel, Y. A. (1998). *Heat Transfer: A Practical Approach*. New York: McGraw-hill.
5. Figes, (2024). Batarya termal yönetim sistemi. Access address: <https://figes.com.tr/matlab-simulink/probleminizi-nasil-cozeceginizi-kesfedin/batarya-termal-yonetim-sistemi>. Access date: 20.09.2024
6. Fong, R., Von Sacken, U., & Dahn, J. R. (1990). Studies of lithium intercalation into carbons using nonaqueous electrochemical cells. *Journal of The Electrochemical Society*, 137(7), 2009. doi:10.1149/1.2086855
7. Ghiji, M., Novozhilov, V., Moinuddin, K., Joseph, P., Burch, I., Suendermann, B., & Gamble, G. (2020). A review of lithium-ion battery fire suppression. *Energies*, 13(19), 5117. doi:10.3390/en13195117
8. Hanley, S. (2023). Condensed Matter Battery From CATL Targets Electric Airplanes. CleanTechnica. Access address: <https://cleantechnica.com/2023/04/21/condensed-matter-battery-from-catl-targets-electric-airplanes/> Access date: 20.09.2024
9. Sezer, K. C., & Basmacı, G. (2022). Şarj edilebilir pillere genel bakış. *Mühendislik Bilimleri ve Tasarım Dergisi*, 10(1), 297-309. doi:10.21923/jesd.946769
10. Kim, B. R., Nguyen, T. N., & Park, C. W. (2023). Cooling performance of thermal management system for lithium-ion batteries using two types of cold plate: Experiment and

- MATLAB/Simulink-Simscape simulation. *International Communications in Heat and Mass Transfer*, 145, 106816. doi:10.1016/j.icheatmasstransfer.2023.106816
11. Kumar, A., Chandekar, A., Deshmukh, P. W., & Ugale, R. T. (2023). Development of electric vehicle with permanent magnet synchronous motor and its analysis with drive cycles in MATLAB/Simulink. *Materials Today: Proceedings*, 72, 643-651. doi:10.1016/j.matpr.2022.08.304
 12. Li, M., Lu, J., Chen, Z., & Amine, K. (2018). 30 years of lithium-ion batteries. *Advanced Materials*, 30(33), 1800561. doi:10.1002/adma.201800561
 13. Lin, J., Chu, H. N., Monroe, C. W., & Howey, D. A. (2022). Anisotropic thermal characterisation of large-format lithium-ion pouch cells. *Batteries & Supercaps*, 5(5), e202100401. doi:10.1002/batt.202100401
 14. Matlab, (2024), Access address: <https://www.mathworks.com/help/simscape-battery/> Access date: 20.09.2024
 15. Monika, K., & Datta, S. P. (2022). Comparative assessment among several channel designs with constant volume for cooling of pouch-type battery module. *Energy Conversion and Management*, 251, 114936. doi:10.1016/j.enconman.2021.114936
 16. Panchal, S., Dincer, I., Agelin-Chaab, M., Fraser, R., & Fowler, M. (2017). Transient electrochemical heat transfer modeling and experimental validation of a large sized LiFePO₄/graphite battery. *International Journal of Heat and Mass Transfer*, 109, 1239-1251. doi:10.1016/j.ijheatmasstransfer.2017.03.005
 17. Fu, P., Zhao, L., Wang, X., Sun, J., & Xin, Z. (2023). A Review of cooling technologies in lithium-ion power battery thermal management systems for new energy vehicles. *Processes*, 11(12), 3450. doi:10.3390/pr11123450
 18. Qian, Z., Li, Y., & Rao, Z. (2016). Thermal performance of lithium-ion battery thermal management system by using mini-channel cooling. *Energy Conversion and Management*, 126, 622-631. doi:10.1016/j.enconman.2016.08.063
 19. White, F. M., & Xue, H. (2003). *Fluid mechanics* (Vol. 3). New York: McGraw-hill.
 20. Yu, S., Mao, Y., Xie, J., Xu, C., & Lu, T. (2024). Thermal runaway chain reaction determination and mechanism model establishment of NCA-graphite battery based on the internal temperature. *Applied Energy*, 353, 122097. doi:10.1016/j.apenergy.2023.122097
 21. Zhang, H., Yang, Y., Ren, D., Wang, L., & He, X. (2021). Graphite as anode materials: Fundamental mechanism, recent progress and advances. *Energy Storage Materials*, 36, 147-170. doi:10.1016/j.ensm.2020.12.027